

Highlights

Development of an Extensible Unified Control System Using the STARS Framework and Common Commands for Detector Control

Ryutaro NISHIMURA, Yuki SHIBAZAKI, Daisuke WAKABAYASHI, Yoshio SUZUKI, Keiichi HIRANO, Hiroaki NITANI, Takashi KOSUGE, Noriyuki IGARASHI

- Unified control system developed for 2-FZPs zooming optics.
- Proposed system based on STARS framework and common commands for detector control.
- The control system is tested at the AR-NE1A beamline in KEK, Japan.

Development of an Extensible Unified Control System Using the STARS Framework and Common Commands for Detector Control*

Ryutaro NISHIMURA^{a,b,*}, Yuki SHIBAZAKI^{a,b}, Daisuke WAKABAYASHI^{a,b},
Yoshio SUZUKI^a, Keiichi HIRANO^{a,b,c}, Hiroaki NITANI^a, Takashi KOSUGE^a and
Noriyuki IGARASHI^{a,b}

^a*Institute of Materials Structure Science, High Energy Accelerator Research Organization (KEK), Tsukuba, 305-0801, Ibaraki, Japan*

^b*Materials Structure Science Program, Graduate Institute for Advanced Studies, Graduate University for Advanced Studies (SOKENDAI), Tsukuba, 305-0801, Ibaraki, Japan*

^c*Graduate School of Pure and Applied Sciences, Tsukuba, 305-8571, Ibaraki, Japan*

ARTICLE INFO

Keywords:
Beamline Control
Zooming Optics
FZP
X-ray
STARS

ABSTRACT

Two Fresnel zone plates zooming optics have been successfully developed and installed at the AR-NE1A beamline of the Photon Factory at the high energy accelerator research organization (KEK) in Japan. To ensure the reliable and versatile operation of this optical instrumentation, a dedicated control architecture has been implemented based on the simple transmission and retrieval system (STARS) framework, incorporating the newly proposed STARS common commands for detector control (CCDC)—a detector-specific data acquisition (DAQ) state and command system. This system serves as both a practical control system for zooming optics and a demonstration model for modular extensibility using the STARS framework and interoperability among detector systems enabled by the CCDC command set. The system has been commissioned, and its performance has been verified at the AR NE1A beamline. The control architecture affords enhanced configurational flexibility for optical components and provides an interface appropriate for both routine users and advanced experimental protocols.

1. Introduction

Synchrotron radiation facilities, including the Photon Factory (PF), High Energy Accelerator Research Organization (KEK), Japan, continuously advance their optical systems to fulfil the growing demand for high-precision X-ray experiments. As these optical components advance in complexity, the collective focus has gradually shifted from the development of primitive individual control systems requiring user expertise toward the development of reliable and user-friendly integrated control systems to ensure stable operation and accommodate a wider range of experimental conditions. However, available human resources are limited for maintaining control systems. It is necessary to achieve labor-saving while accommodating diverse equipment and experimental methods, promoting standardization, where feasible, and adopting a modular design for control systems. These features facilitate reconfiguration and reuse. Examples of control frameworks that address these requirements are DAQ-Middleware [1, 2] (mainly used in neutron experiments and muon experiments at J-PARC [3] MLF [4]), MADOCA [5] (mainly used at SPring-8 [6] and NanoTerasu [7]), EPICS [8, 9] (mainly used for controlling large accelerators in large accelerator facilities such as J-PARC, SuperKEKB [10] and LANSCE [11]), TANGO [12] (mainly used at synchrotron radiation facilities in Europe such as ESRF [13]) and TINE [14] (mainly used for accelerator control system at DESY [15]). In the PF beamlines, the simple transmission and retrieval system (STARS) framework [16, 17] have been mainly used. Although differences exist depending on the facility's specific circumstances, these frameworks share a common structure: modules divided by function or device are interconnected via communication protocols such as TCP/IP to exchange information. This structure facilitates easy reconfiguration and the reutilization of developed modules, offering excellent scalability. Furthermore, it enables the sharing of development assets within each facility as well as between facilities through the community. By contrast, the methods for linking modules differs depending on the framework. They can be

*

*Corresponding author

✉ ryutaro.nishimura@kek.jp (R. NISHIMURA)
ORCID(s): 0000-0002-3156-7347 (R. NISHIMURA)

1

broadly categorized into two types: stateful designs that manage all modules using common commands and shared data acquisition (DAQ) states and stateless designs, where each module has its own commands and does not share common DAQ states. Generally, in stateful designs, the control mechanisms of each module are standardized, and thus, the differences between devices are inherently absorbed. However, because strict DAQ state management and precise control of DAQ state transition sequences between modules are required, the scalability of stateful designs tends to be lower than that of stateless designs. STARS is characterized by a stateless design owing to the minimal requirement for all components within the beamline framework to share a uniform DAQ state. This design choice prioritizes flexibility for reconfiguration, accommodating frequent modifications in experimental apparatus and measurement methodologies. Notably, the stateless design of STARS is advantageous for advancing the beamline owing to its low design cost. However, in this design, the device-specific control system is reflected in the module control commands, which is a major drawback and necessitates a comprehensive overhaul of the control system when replacing similar devices. To address this issue, we propose introducing dedicated DAQ states for certain experimental devices when frequent replacements are anticipated. This approach would enable minimal control using only common commands from the STARS framework. Additionally, it is expected to enable easier replacement and the utilization of devices of the same type, whose characteristics differ from those of their predecessors. This method allows the construction of measurement systems that have better leverage the high scalability of STARS, which has already been widely deployed in the PF.

Thus, we developed a new unified control framework as a model system using dedicated DAQ states. This model system demonstrates modular expandability by leveraging the STARS framework and inter-operability between detectors through the proposed STARS common commands for detector control (CCDC), which is a detector-specific DAQ state and command system. This system provides enhanced flexibility for optical-configuration changes and an intuitive interface that supports both routine users and advanced experimenters. Simultaneously, this system is developed as a practical control system for zooming optics using two Fresnel zone plates (FZPs) [18] installed in the AR-NE1A beamline in the PF. Therefore, in this study, we verified the effectiveness of the proposed system through automated measurement tests by combining the control of the two FZPs (2-FZPs) zooming optics using STARS with detector control via CCDC.

2. Overview of Zooming X-ray Microscope at AR-NE1A

2.1. 2-FZPs Zooming Optics

The 2-FZPs zooming optics [18] (Figure 1) enables X-ray microscopy zooming by adjusting the FZP positions while maintaining a fixed camera length (the object-to-camera distance). This optics, allowing wide-range magnification (approximately 25 \times to 300 \times) with a short camera length (approximately 6.9 m), was initially installed at the PF AR-NE1A beamline [19]. The X-ray beam from a multipole wiggler is monochromatized through a Si 111 double-crystal monochromator and collimated by variable-bent double multilayer mirror optics in a crossed-mirror geometry (Kirkpatrick-Baez optics) to achieve parallel beam illumination. The beam passes through the aperture and illuminates the sample, with only the lower half of FZP1 irradiated for diffraction-order sorting. The X-ray beam passing through the sample is magnified by FZP1 and further magnified by FZP2 in the high-magnification mode. The FZPs (made by Applied Nanotools, Inc.) have a diameter of 550 μm and Au zones with a thickness of more than 600 nm. The outermost zone widths Δr_n of FZP1 and FZP2 are 25 and 50 nm, respectively. For schlieren phase contrast imaging, the beam is partially cut-off by a knife edge at the back focal plane of FZP1. The beam travels through a 5-m vacuum pipe and is captured by the X-ray camera, with the camera length set to 6.9 m.

2.2. Labor Involved in Optical Control

Although the 2-FZPs zooming optical system has a relatively simple configuration, adjusting the positions of the optical elements, such as FZPs, apertures, and knife edges, is essential when changing the magnification. Furthermore, the position of the sample stage must be adjusted for appropriate measurements. To adjust these elements, up to 32 motorized stages, related to the position of each element, must be controlled. Additionally, the upstream monochromator and multilayer mirrors (controlled by up to 16 motorized stages) must be adjusted when changing the X-ray energy, depending on the desired magnification and sample type. Therefore, developing a control system, with a user interface that enables easier control for users who are not beamline experts, is necessary.

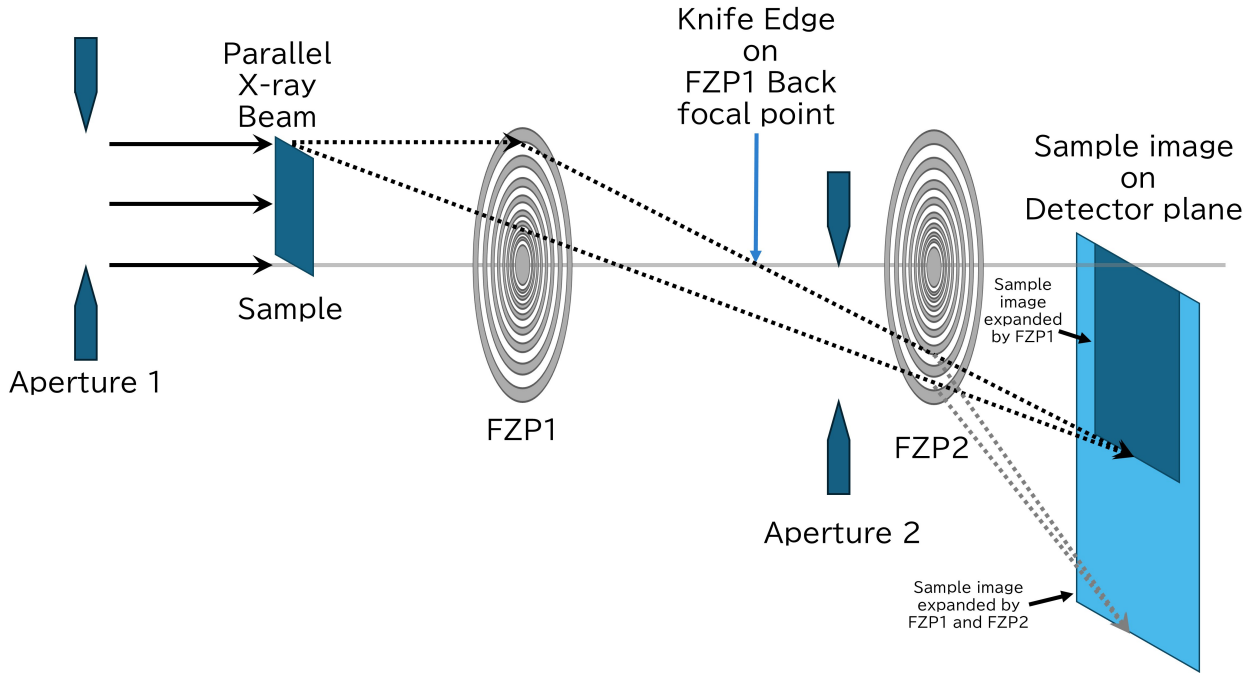


Figure 1: Schematic of the 2-FZPs zooming optics. In this optical system, positional adjustment of FZP2 (including removing FZP2 from the optical path) enables a wide range of variable magnification even with a short camera length. Here, the low magnification mode using only FZP1 is termed 1-FZP mode, and the high magnification mode using both FZP1 and FZP2 is termed 2-FZPs mode. Furthermore, inserting a knife edge at the back focal position of the FZP1 allows the acquisition of a Schlieren contrast image.

2.3. Detector Selectivity

The X-ray energy in this optical system varies based on the desired magnification and sample type. The field of view, resolution, and other parameters differ for different target samples. Because a single detector cannot cover all sample and measurement conditions, different detectors must be used. Thus, the control system needs detector control functionality for easy switching between detectors.

3. Proposed New Control System

To address these requirements, we developed a new control system. This section describes the key technologies used in the new system and provides an overview of the same.

3.1. STARS Framework

STARS [16, 17] is a message transferring framework for equipment control in the PF beamlines. This framework, designed for smallscale control systems with standard TCP/IP sockets, can be applied to various types of operating systems. It also enables the development of control/measurement modules using various programming languages capable of handling TCP/IP sockets.

This framework consists of client programs called STARS clients and a server program called STARS server, and each STARS client is connected to the STARS server via a TCP/IP (figure 2). The STARS clients and server process only text-based messages, which can support structured data in JavaScript Object Notation (JSON), Extensible Markup Language (XML), and plain text. Each STARS client has a unique node name and sends messages to the server with the destination node name. STARS clients can have subnodes, and commands can be sent directly between nodes by specifying the destination; this operation enables easy construction of hierarchical systems.

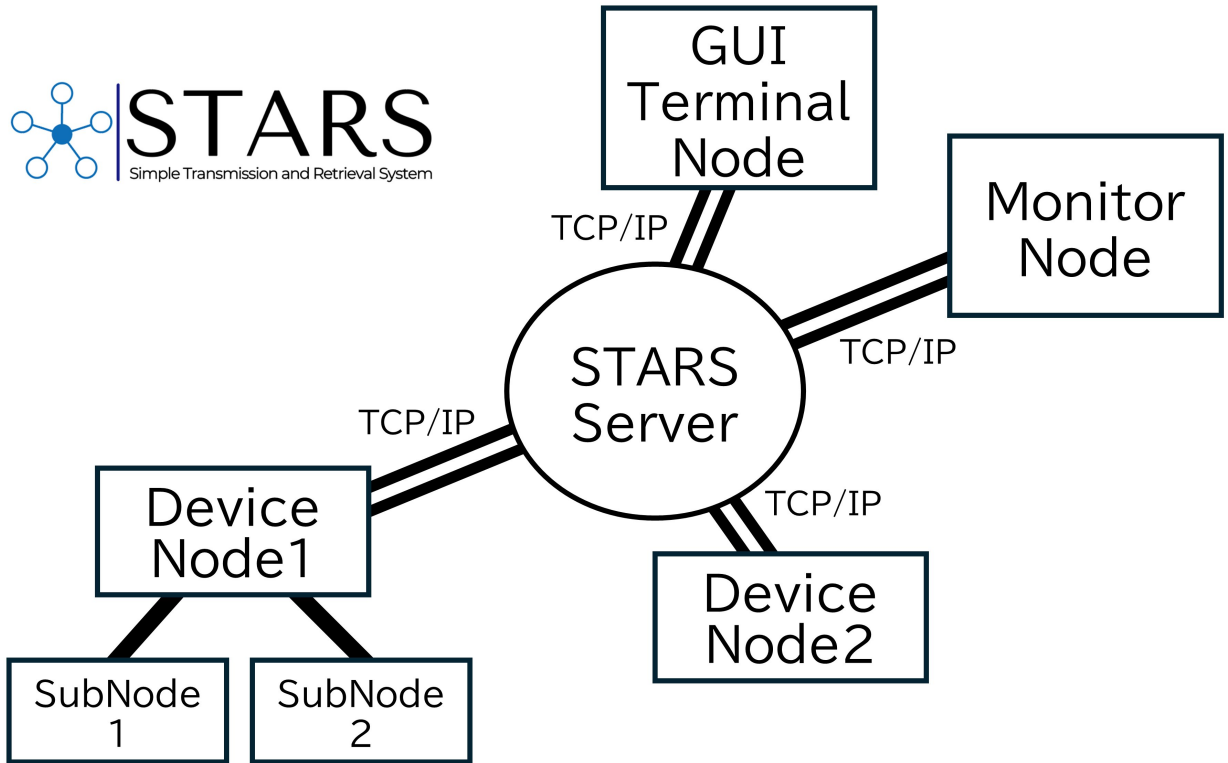


Figure 2: Schematic of the STARS framework. This framework consists of client programs called STARS clients (Device Node 1, Device Node 2, GUI Terminal Node, and Monitor Node in this figure) and a server program called STARS server (in the center of this figure), and each STARS client is connected to the STARS server via a TCP/IP.

3.2. STARS CCDC

STARS CCDC [20] is the detector command system for achieving basic control using STARS. It enhances the inter-operability between the detectors, enabling the selection of detectors suited to specific measurement conditions without requiring major modifications to the measurement system.

In X-ray imaging, different detectors may be selected depending on the measurement sample, optical system, and X-ray energy. In these detectors, the commands and parameters used for control are specific to each detector and are fundamentally incompatible. Consequently, when performing automated measurements encompassing the optical system and peripheral equipment, adapting to each detector is challenging. Therefore, in CCDC, instead of directly implementing the control commands and parameters for each detector within the detector control STARS client, the minimum control commands and transmission parameters required to measure one set of data (e.g., one image) are abstracted, encapsulating the detector-specific commands and parameters. This process enables detector switching without requiring modifications to the measurement control system. Specifically, it is implemented using the seven DAQ states shown in Figure 3 and six DAQ transition commands that transition between these DAQ states. The seven DAQ states correspond to the following situations; upon the launch of the detector control, the client supporting CCDC always enters the “DAQ_Deinitialized” state initially.

DAQ_Deinitialized Initial state upon software launch. In this state, no specific preparation is made for the detector hardware, including connections.

DAQ_Initialized Initialization completed state. In this state, a detector hardware connection is guaranteed to have been established.

DAQ_Configured State in which the parameter settings for using the detector are completed.

DAQ_Calibrating State in which the detector calibration is in progress.

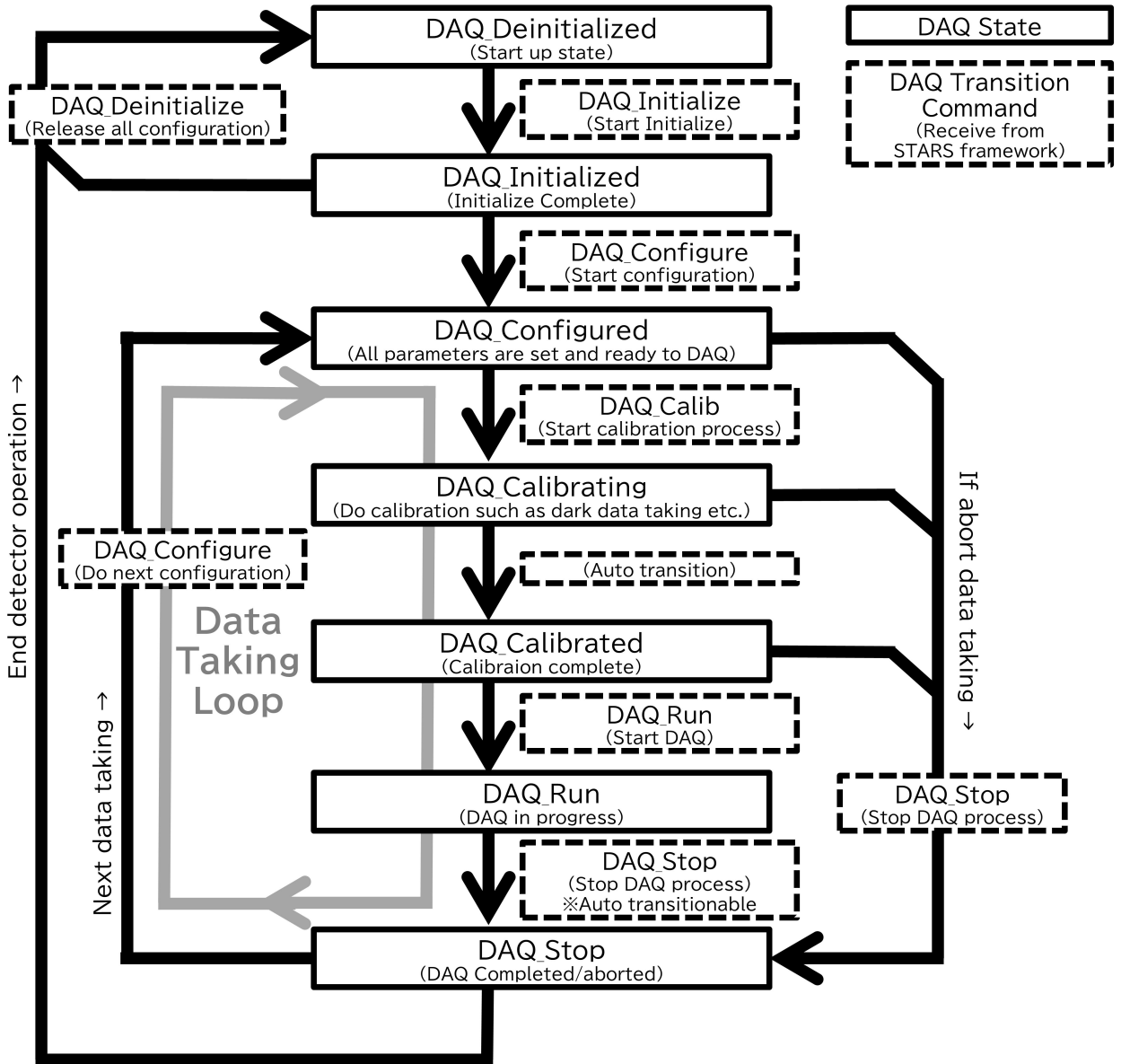


Figure 3: Schematic of STARS CCDC in the detector control STARS client. The detector control client supporting CCDC implements six minimal control commands and seven DAQ states. The seven DAQ states each denote the following situations: **DAQ_Deinitialized** – Initial state upon software launch. **DAQ_Initialized** – State of initialization completed. **DAQ_Configured** – State in which the parameter settings for using the detector are completed. **DAQ_Calibrating** – State when detector calibration is in progress. **DAQ_Calibrated** – This state indicates that the detector calibration is complete, and operational measurements can be performed. **DAQ_Run** – A state describing the actual measurement by the detector is currently in progress. **DAQ_Stop** – This state indicates that the measurement has stopped.

DAQ_Calibrated This state indicates that the detector calibration is complete, and operational measurements can be performed.

DAQ_Run A state describing the ongoing actual measurement by the detector .

DAQ_Stop This state indicates that the measurement has stopped.

Completing one set of data acquisition involves cycling through the DAQ states from DAQStart to DAQStop (“Data taking loop” in Figure 3). To acquire multiple sets, we simply transition through the DAQ states the required number of times. Note that these DAQ states defined by CCDC are intended to enable mutual interpretation of the DAQ states and commands when the detector control software requires multiframework compatibility.

When developing CCDC-implemented STARS clients for each detector, developers must organize detector-specific commands and parameters into categories that should be executed and transmitted at each DAQ state. This categorization should be implemented to process them appropriately according to the DAQ state transitions. To maintain inter-operability, the DAQ state and transition commands are fixed and cannot be changed. However, other commands, such as detector-specific parameter settings, may be implemented as desired. When implementing commands, developers must ensure that measurements using DAQ transition commands remain feasible after the detector parameters are configured on the client. For certain parameters, such as exposure time settings, recommended command name is prepared.

Currently, the DAQ software (implemented STARS client interface), developed in KEK for the Hamamatsu sCMOS detector C12849-111U [21], INTPIX4NA SOIPIX detector [22, 23], GPixel GSENSE400BSI-PS-based soft X-ray sCMOS detector [24], and Dectris Eiger2X detector [25], supports CCDC. Additionally, this software can support other detectors in the future.

3.3. Overview of the Proposed New Control System

Our new control system is constructed using the STARS framework and CCDC. Figure 4 presents a schematic of the system. In this system, the management of the optical system, which pertains to up to 32 motorized stages, and the control of the detector is executed via independent modules functioning as STARS clients. Each module is interconnected through the STARS server. Additionally, to control upstream components such as monochromators and mirrors required for X-ray energy control (controlled by up to 16 motorized stages), this system is relay-connected to the existing STARS-based control system. The user can control and perform measurements via a unified control graphical user interface (GUI) module, which enables integrated control with existing control systems. This unified control GUI module incorporates various adjustments and automatic measurement algorithms described below, and is coded with an objective structure designed to facilitate partial or complete adaptation to other systems in the future.

In this system, users can select detectors that support CCDC for each experimental condition. The Hamamatsu sCMOS detector C12849-111U [21] and INTPIX4NA SOIPIX detector [22, 23] are available for use. The Hamamatsu sCMOS detector C12849-111U has a pixel format of 2048×2048 , a pixel size of $6.5 \mu\text{m}$, a $10\text{-}\mu\text{m}$ -thick gadolinium oxysulfide (P43) scintillator, and 1:1 fiber optics. This detector employs a scintillator and is an indirect conversion-type device, providing resolution characteristics inferior to those of direct conversion detectors. However, the scintillator captures high-energy X-rays with high penetrating power, and the detector circuitry is relatively resistant to radiation damage. Consequently, it is well-suited for imaging under conditions where the X-ray intensity is relatively high at comparatively high X-ray energies (for example, 14.4 keV in this optical system). The INTPIX4NA SOIPIX detector has a pixel format of 832×512 , pixel size of $17 \mu\text{m}$, and $320\text{-}\mu\text{m}$ -thick high-resistivity silicon substrate for X-ray detection. This direct conversion-type detector with a silicon substrate facilitates X-ray detection, offering excellent sensitivity and resolution characteristics. It is well-suited for imaging under conditions where the X-ray intensity is relatively low at comparatively low X-ray energies (for example, 9.6 keV with this optical system). This system adjusts the optical and upstream components to predetermined positions using precalibrated preset values according to the energy specified by the user from a GUI. This adjustment enables users to commence measurements promptly without expending considerable effort or time to adjust the energy or optics for each experiment. Additionally, this system has several semi-automated control and measurement functions, as explained here.

Energy and Optics Switching This function enables semiautomatic switching of the X-ray energy and zooming optics tuning using pre-prepared preset values. This feature is necessary for the following reasons.

1. The magnification of this optics is determined by the energy of the X-rays. For example, the magnification at 14.4 keV is approximately $25\times$ to $150\times$, whereas at 9.6 keV , it is approximately over $300\times$ [18]. At high energies, lower magnification can be used, whereas at low energies, higher magnification can be used. By switching the energy of the X-rays, observations can be performed across a wide range of magnifications that cannot be covered by a single X-ray energy.
2. Depending on the sample and measurement conditions, high X-ray transmission may be required. For instance, with samples exhibiting high absorption, such as those with considerable thickness or containing

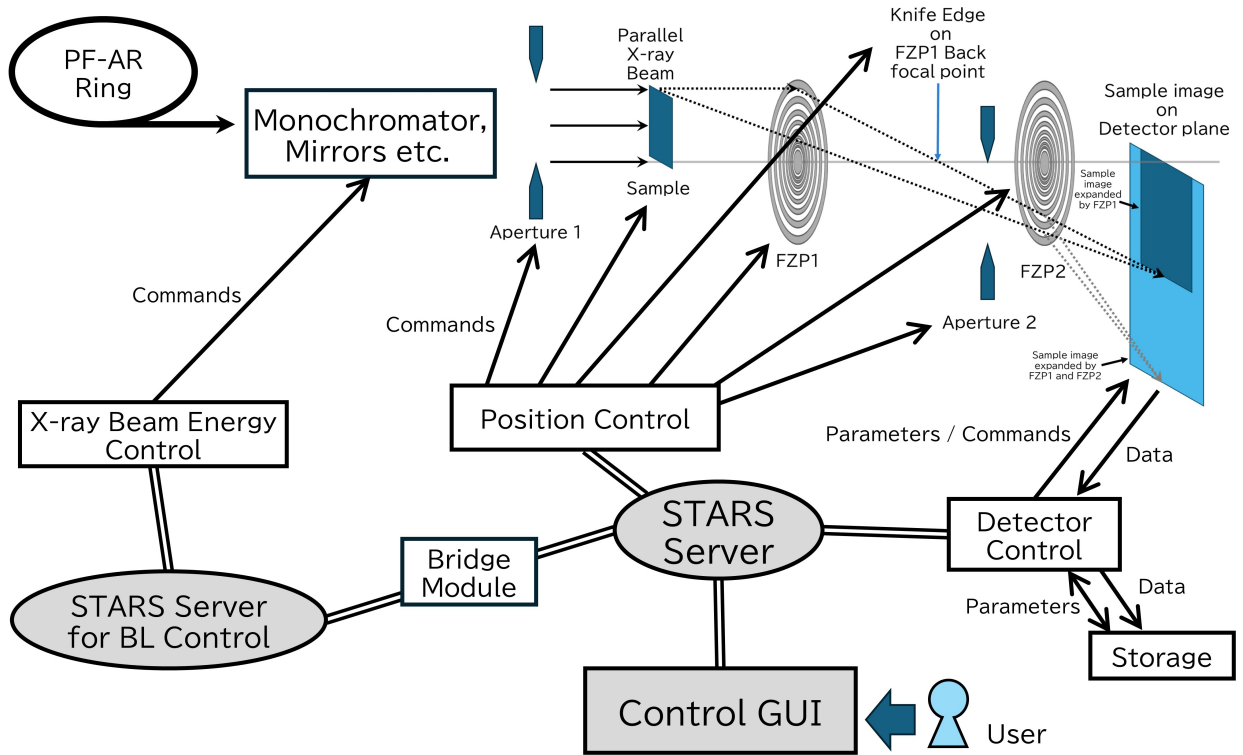


Figure 4: Schematic of proposed new control system. In this system, the control of the optical system and the control of the detector are implemented as independent modules as STARS clients, and each module is interconnected via the STARS server. This system is relay-connected to the existing STARS based control system for upstream components such as monochromators and mirrors required for X-ray energy control. The user control and performs measurements via a unified control GUI.

heavy elements, high-energy X-rays with high penetrating power must be employed. Furthermore, when observing thin samples at maximum magnification, low-energy X-rays must be used, even if the transmission efficiency is reduced.

One Shot Imaging This is a simple method for acquiring one image without any peripheral control. This function sequentially issues commands to the cycle through the DAQ states of CCDC. The actual behavior depends on the implementation of the detector-side software.

Focus Check In this measurement, data for optical-system focus adjustment are captured. This function executes a process that changes the position of the FZP or sample in predetermined steps, performs imaging, and records a set of positional information and images.

Two-Dimensional Multishot In this measurement, the sample is repeatedly moved in predetermined steps, and images are captured. This function enables the imaging of samples with sizes larger than the field of view. Using this approach, the user can specify separate displacement values and step counts for the horizontal and vertical movement of the sample. The acquired images can be stitched together into a single large image using software processing.

Computed Tomography / Laminography Data Taking In this measurement, datasets for computed tomography or laminography are acquired. For this measurement, an X-ray profile image, called I_0 , is acquired for normalization. After positioning the sample, it is rotated in predetermined angular steps, and an image is captured at each step, yielding a dataset covering 180° or 360°.

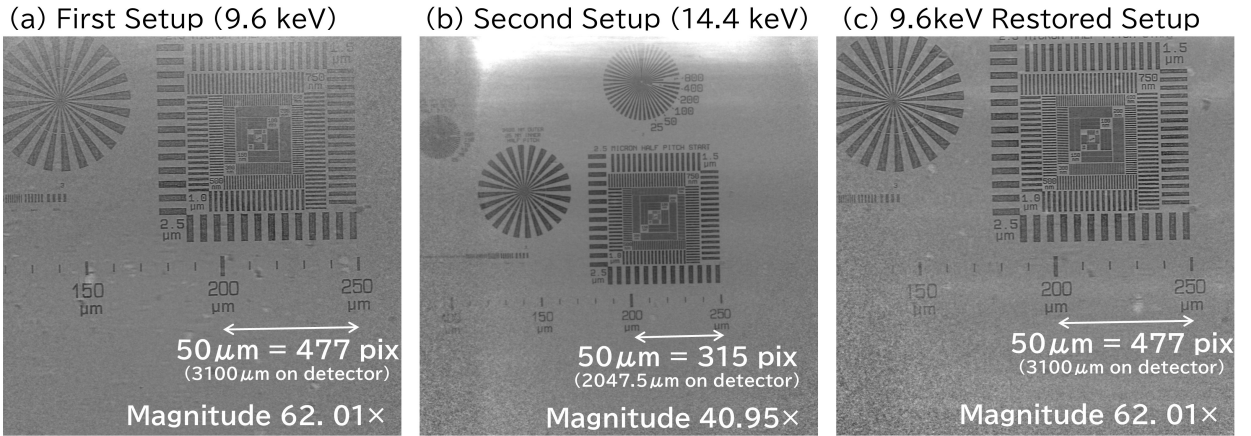


Figure 5: Test result of energy and optics switching. Test pattern images recorded by the Hamamatsu sCMOS detector C12849-111U and normalized by the X-ray beam profile. (a) First setup with 9.6 keV monochromatic X-ray condition. Magnitude is 61.01 \times . This condition is stored in the control system. (b) Second setup with 14.4 keV monochromatic X-ray condition. Magnitude is 40.95 \times . (c) 9.6 keV monochromatic X-ray condition restored from the previous 14.4 keV condition by the control system.

4. Demonstration of Measurements

A set of measurements were performed using the developed control system. The experimental setup of the X-ray microscope was installed at the AR-NE1A beamline of the PF facility at KEK. In these measurements, a Hamamatsu sCMOS detector C12849-111U and an INTPIX4NA SOIPIX detector were used. The test pattern employed as a demonstration sample, specifically the Siemens star and line-and-space patterns, served as the calibration standard (CAL21HEI2, Applied Nanotools) and was composed of 600-nm-thick Au.

4.1. Energy and Optics Switching

In this measurement, energy switching was performed in the following sequence: First, the optical system was tuned to the X-ray energy of 9.6 keV to create a preset. Second, the energy was changed to 14.4 keV, and the optical system was retuned. Finally, the energy was switched to the initial 9.6 keV preset value to confirm the restoration of the optical system's state. This measurement was performed in the 1-FZP mode. Figure 5 presents the measurement results obtained using the Hamamatsu sCMOS detector (C12849-111U). Figures 5 (a), (b), and (c) show images of the test patterns recorded using the 9.6 (preset condition), 14.4, and 9.6 keV (restored) tuned setups, respectively. A comparison of Figures 5 (a) and (c) shows that both the magnification and focus adjustment show precise alignment. These results confirm the proper optical-control functioning of the developed control system.

4.2. Two-Dimensional Multishot

In this case, a continuous automatic measurement was performed (in the 1-FZP mode) in 50 μm steps of 5×5 (25 points) for the test pattern, whose size could not be fully covered by the field of view of the optics. Figure 6 shows a stitched image of the test pattern, obtained from the test result of a 5×5 two-dimensional multishot of the test pattern captured by the INTPIX4NA SOIPIX detector with an X-ray energy of 9.6 keV. Figure 7 displays a stitched image of the test pattern, obtained from a similar test result yielded by the Hamamatsu sCMOS detector C12849-111U with an X-ray energy of 14.4 keV. These stitched images were processed by the grid / collection stitching plugin [26] attached to the Fiji image processing software [27]. For both the detectors, the two-dimensional multishot measurements were performed at a resolution that did not interfere with the stitching process. These results confirm that the control system operates as intended.

4.3. Computed Laminography Data Taking

Continuous automatic measurements were performed at full-circle rotation (0.5° step, 721 datasets) for a small rubbery ball sample in a panoramic diamond anvil cell (DAC). Figure 8 (a) shows the setup for computed laminography. This measurement was performed in the 2-FZPs mode (magnitude = 178 \times) with an X-ray energy of 9.6 keV. The DAC

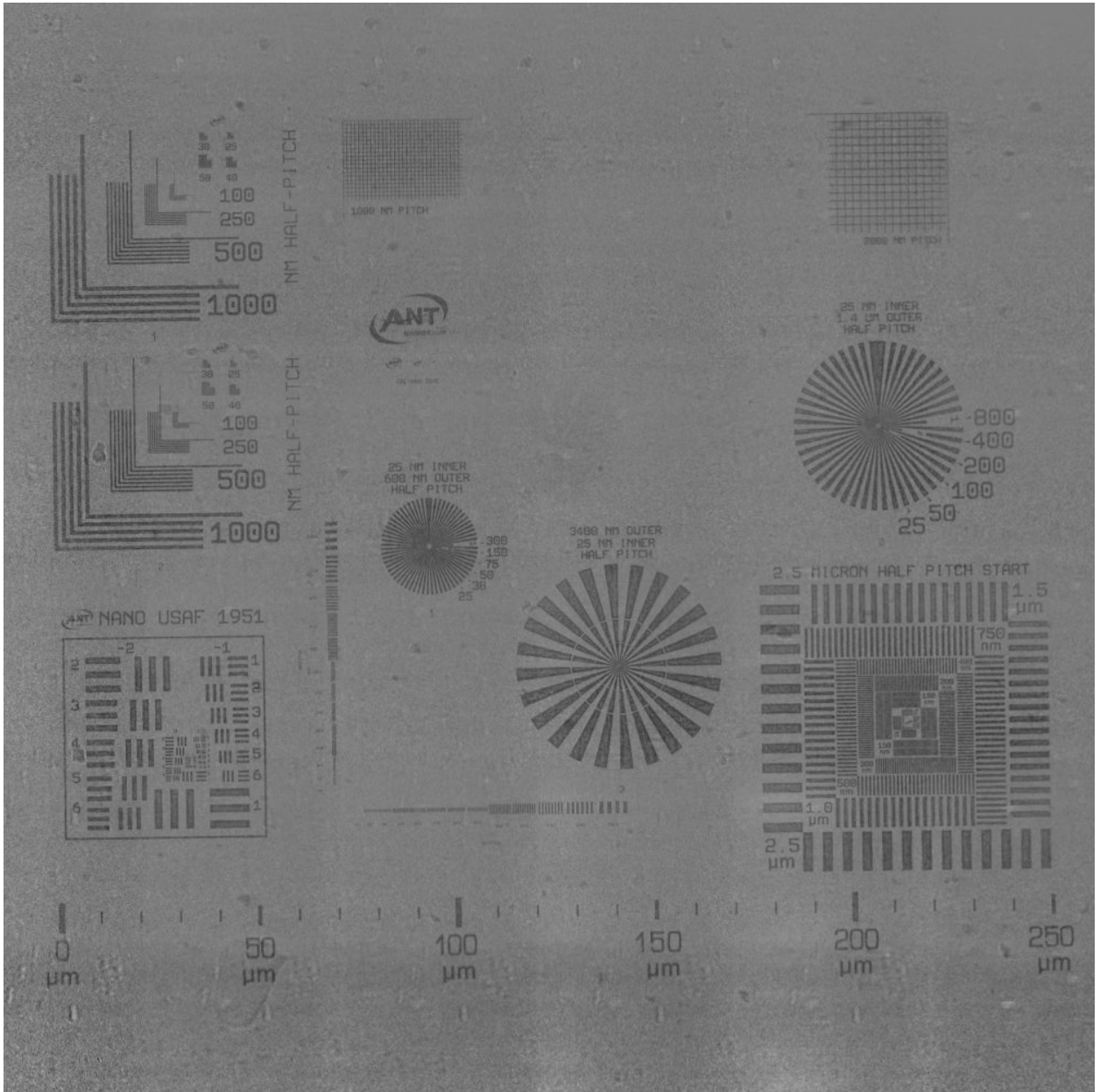


Figure 6: Stitched image from the test result of 5×5 two-dimensional multishot taken by the INTPIX4NA SOIPIX detector with the X-ray energy of 9.6 keV. Image was normalized by X-ray beam profile. This image was processed by the grid / collection stitching plugin attached to Fiji image processing software.

possessed two-fold 300° (150° unobstructed symmetric) radial openings in the horizontal direction. The diamond culet size and applied pressure were $300 \mu\text{m}$ and 10 GPa, respectively. Additionally, the gasket material was W-Re (thickness of $40 \mu\text{m}$), and the hole diameter was $120 \mu\text{m}$. A rubby ball, with a diameter of $15 \mu\text{m}$ and cBN-powder pressure medium, was used as the sample, and the measurements were performed using the INTPIX4NA SOIPIX detector. Figure 8 (b) shows a shot of the small rubby ball sample, placed inside the DAC, extracted from the acquired laminography dataset. All the data obtained in this study were complete, with no instance of missing data points. These results confirm that the operation of the proposed control system is consistent with its design objectives.

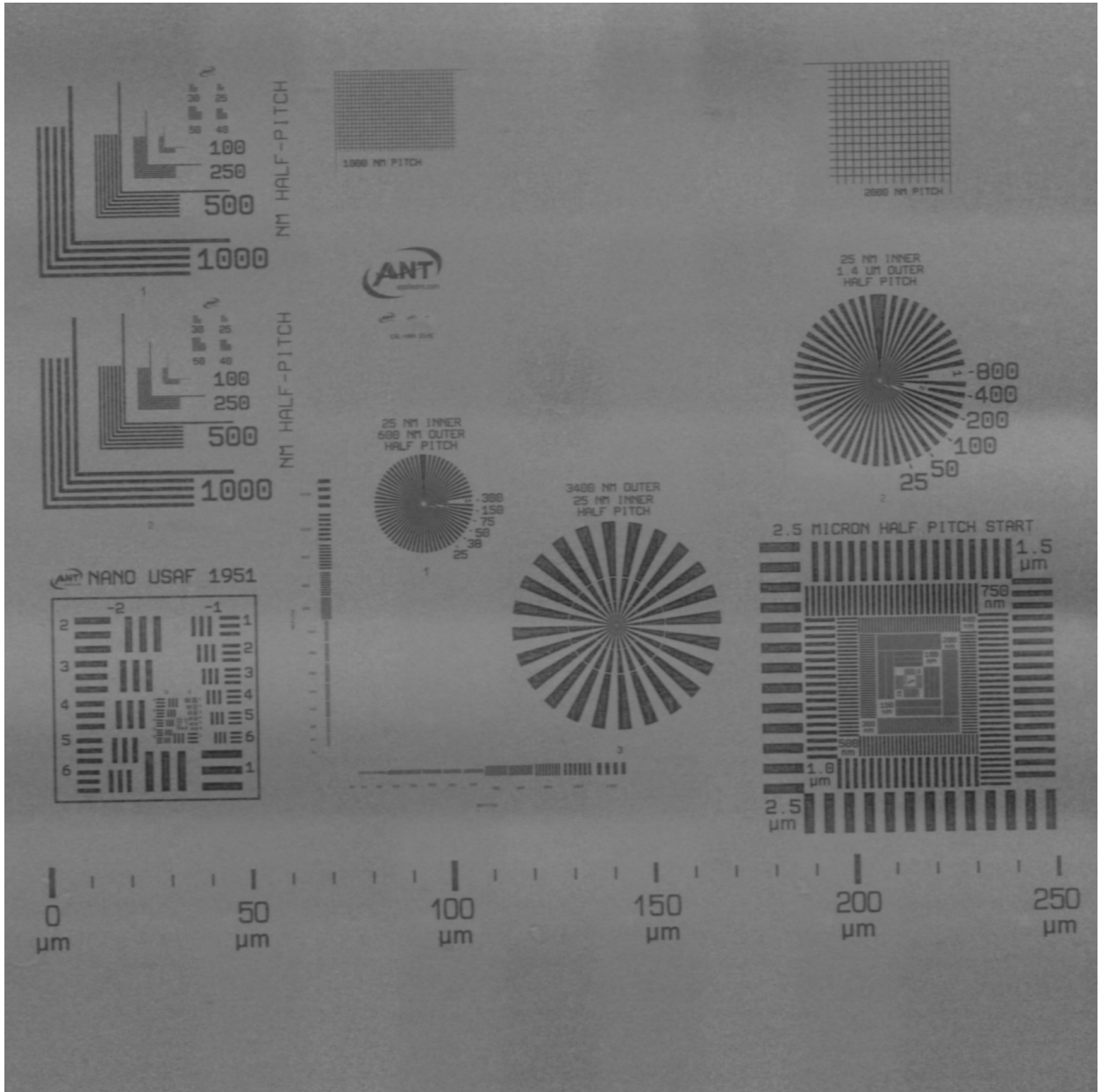


Figure 7: Stitched image from the test result of 5×5 two-dimensional multishot taken by Hamamatsu sCMOS detector C12849-111U with the X-ray energy of 14.4 keV. Image was normalized by X-ray beam profile. This image was processed by the grid / collection stitching plugin attached to Fiji image processing software.

5. Conclusions

A novel unified control system was developed for the 2-FZPs zooming optics, installed in the PF AR-NE1A beamline, as a model system using STARS CCDC— a detector-specific DAQ state and command system. This control system demonstrates modular expandability by leveraging the STARS framework and inter-operability between detectors through the proposed STARS CCDC. This control system was also designed as a practical system to facilitate user access to these optics. The operation of the developed system was demonstrated using an actual optics setup in the PF AR-NE1A beamline, and the results confirmed that it operated as intended. Access to this system will be granted to users in the near future, and we intend to implement further enhancements based on the feedback received from users.

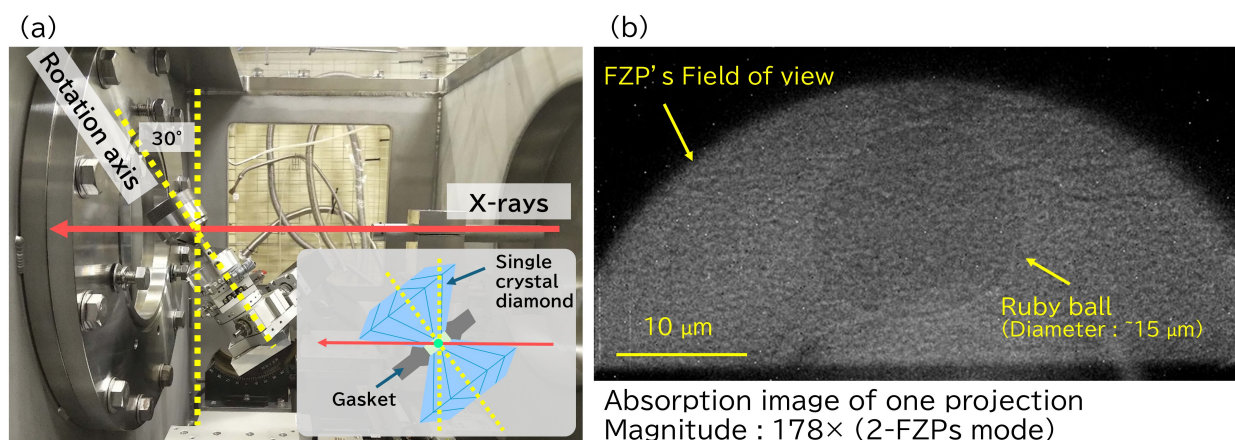


Figure 8: (a) Setup of computed laminography. (b) One shot of the small rubby ball sample in the DAC, extracted from the acquired laminography dataset.

Moreover, the STARS-based optical integration control system and CCDC developed in this study can be readily applied to other systems. Their utilization is anticipated in multiprobe measurements (e.g., X-rays, muons, neutrons, and lasers); such measurements are expected to be conducted extensively in the future. Furthermore, their application is anticipated in next-generation planned facilities, such as the Multi Quantum-Beam Facility with Superconducting Linac for Material-Quantum-Life Sciences [28].

6. Acknowledgements

This study was conducted at the AR-NE1A beamline of the Photon Factory facility at KEK (Proposal No. 2021PF-S001, 2024PF-G006, 2025PF-G004 and 2025PF-G016).

CRedit authorship contribution statement

Ryutaro NISHIMURA: Conceptualization of this study, Data curation, Formal analysis, Investigation, Methodology, Software, Visualization, Writing - original draft preparation, Writing - review and editing. **Yuki SHIBAZAKI:** Data curation, Funding acquisition, Investigation, Resources, Supervision, Validation, Writing - review and editing. **Daisuke WAKABAYASHI:** Data curation, Funding acquisition, Investigation, Resources, Supervision, Validation, Writing - review and editing. **Yoshio SUZUKI:** Data curation, Supervision, Validation, Visualization, Writing - review and editing. **Keiichi HIRANO:** Data curation, Funding acquisition, Resources, Supervision, Validation, Writing - review and editing. **Hiroaki NITANI:** Data curation, Funding acquisition, Investigation, Project administration, Resources, Supervision, Validation, Writing - review and editing. **Takashi KOSUGE:** Data curation, Funding acquisition, Investigation, Resources, Supervision, Validation, Writing - review and editing. **Noriyuki IGARASHI:** Data curation, Funding acquisition, Investigation, Project administration, Resources, Supervision, Validation, Writing - review and editing.

References

- [1] Y. Yasu, K. Nakayoshi, E. Inoue, H. Sendai, H. Fujii, N. Ando, T. Kotoku, S. Hirano, T. Kubota, T. Ohkawa, A Data Acquisition Middleware, in: 2007 15th IEEE-NPSS Real-Time Conference, pp. 1–3.
- [2] Y. Yasu, K. Nakayoshi, H. Sendai, E. Inoue, Functionality of DAQ-Middleware, IEEE Transactions on Nuclear Science 57 (2010) 487–490.
- [3] J-PARC Center, J-PARC | Japan Proton Accelerator Research Complex, <https://j-parc.jp/c/en/index.html>, Accessed on 05/03/2026.
- [4] J-PARC MLF, J-PARC MLF (Materials and Life Science Experimental Facility), <https://mlfinfo.jp/en/>, Accessed on 05/03/2026.
- [5] R. Tanaka, T. Fukui, Y. Furukawa, T. Hatsui, T. Hirono, N. Hosoda, M. Ishii, M. Kago, A. Kiyomichi, H. Maesaka, T. Masuda, T. Matsumoto, T. Matsushita, T. Ohata, T. Ohshima, T. Otake, Y. Otake, C. Saji, T. Sugimoto, T. Takebe, M. Yamaga, A. Yamashita, First operation of the sacra control system in spring-8, in: 2011 2nd International Particle Accelerator Conference.
- [6] RIKEN/JASRI, SPring-8 Web Site, <http://www.spring8.or.jp/en/>, Accessed on 05/03/2026.
- [7] QST, NanoTerasu | 3 GeV Synchrotron Radiation Facility in Japan, https://nanoteranu.jp/top_en/, Accessed on 05/03/2026.

- [8] Fritz-Haber-Institut der Max-Planck-Gesellschaft, EPICS - Experimental Physics and Industrial Control System, <https://epics-controls.org/>, Accessed on 05/03/2026.
- [9] Argonne National Laboratory, EPICS Home at Argonne, <https://epics.anl.gov/>, Accessed on 05/03/2026.
- [10] Y. Ohnishi, T. Abe, T. Adachi, K. Akai, Y. Arimoto, K. Ebihara, K. Egawa, J. Flanagan, H. Fukuma, Y. Funakoshi, K. Furukawa, T. Furuya, N. Iida, H. Inuma, H. Ikeda, T. Ishibashi, M. Iwasaki, T. Kageyama, S. Kamada, T. Kamitani, K. Kanazawa, M. Kikuchi, H. Koiso, M. Masuzawa, T. Mimashi, T. Miura, T. Mori, A. Morita, T. Nakamura, K. Nakanishi, H. Nakayama, M. Nishiwaki, Y. Ogawa, K. Ohmi, N. Ohuchi, K. Oide, T. Oki, M. Ono, M. Satoh, K. Shibata, M. Suetake, Y. Suetsugu, R. Sugahara, H. Sugimoto, T. Suwada, M. Tawada, M. Tobiyama, N. Tokuda, K. Tsuchiya, H. Yamaoka, Y. Yano, M. Yoshida, S. Yoshimoto, D. Zhou, Z. Zong, Accelerator design at superkekb, Progress of Theoretical and Experimental Physics 2013 (2013) 03A011.
- [11] Los Alamos National Laboratory, Los Alamos Neutron Science Center, <https://lansce.lanl.gov/>, Accessed on 05/03/2026.
- [12] Tango Controls Steering Committee, TANGO Controls, <https://www.tango-controls.org/>, Accessed on 05/03/2026.
- [13] European Synchrotron Radiation Facility, European Synchrotron Radiation Facility (ESRF), <https://www.esrf.fr/>, Accessed on 05/03/2026.
- [14] P. Bartkiewicz, P. Duval, S. Herb, H. Wu, THE TINE CONTROL SYSTEM, OVERVIEW AND STATUS, in: 2007 11th International Conference on Accelerator and Large Experimental Physics Control Systems.
- [15] Deutsches Elektronen-Synchrotron, Deutsches Elektronen-Synchrotron DESY, https://desy.de/index_eng.html, Accessed on 05/03/2026.
- [16] KEK IMSS Photon Factory, Welcome to STARS, <https://stars.kek.jp/>, Accessed on 25/04/2025.
- [17] T. Kosuge, Y. Saito, RECENT PROGRESS OF STARS, Proc. PCaPAC 2005 (2005).
- [18] D. Wakabayashi, Y. Suzuki, Y. Shibazaki, H. Sugiyama, K. Hirano, R. Nishimura, K. Hyodo, N. Igarashi, N. Funamori, X-ray zooming microscopy with two Fresnel zone plates, Re. Sci. Instrum. 93 (2022) 033701.
- [19] KEK IMSS Photon Factory, AR-NE1A : X-Ray Diffraction and Mössbauer Spectroscopy at High Pressure, <https://www2.kek.jp/imss/pf/eng/apparatus/bl/ne1a.html>, Accessed on 18/11/2025.
- [20] KEK IMSS Photon Factory, STARS Common Commands for Detector Control, https://stars.kek.jp/doku.php?id=stars_common_commands_for_detector_control, Accessed on 18/11/2025.
- [21] K.K. Hamamatsu Photonics, X-ray sCMOS camera C12849-111U, https://www.hamamatsu.com/resources/pdf/sys/SCAS0139E_C12849.pdf, Accessed on 18/11/2025.
- [22] R. Nishimura, S. Kishimoto, T. Sasaki, S. Mitsui, M. Shinya, Y. Arai, T. Miyoshi, "INTPIX4NA" - New integration-type silicon-on-insulator pixel detector for imaging application, J. Instrum. 16 (2021) P08054.
- [23] R. Nishimura, N. Igarashi, D. Wakabayashi, Y. Shibazaki, Y. Suzuki, K. Hirano, Y. Arai, X-ray imaging camera using INTPIX4NA SOIPIX detector with SiTCP-XG 10GbE based high-speed readout system, NIMA 1064 (2024) 169429.
- [24] ARTRAY CO., LTD., Soft X-ray Camera ARTCAM-400SX-USB3, <https://artray.co.jp/en/products/soft-X-rays.html>, Accessed on 18/11/2025.
- [25] DECTRIS AG, EIGER2 X/XE for Synchrotrons, <https://www.dectris.com/en/detectors/x-ray-detectors/eiger2/eiger2-for-synchrotrons/eiger2-x/>, Accessed on 18/11/2025.
- [26] S. Preibisch, S. Saalfeld, P. Tomancak, Globally optimal stitching of tiled 3D microscopic image acquisitions, Bioinformatics 25 (2009) 1463–5.
- [27] J. Schindelin, I. Arganda-Carreras, E. Frise, V. Kaynig, M. Longair, T. Pietzsch, C. Rueden, S. Saalfeld, B. Schmid, J. Y. Tinevez, D. J. White, V. Hartenstein, K. Eliceiri, P. Tomancak, A. Cardona, Fiji: an open-source platform for biological-image analysis, Nat. Methods 9 (2012) 676–682.
- [28] KEK-IMSS, MB-LINQ, <https://www2.kek.jp/imss/mb-linq/>, Accessed on 24/02/2026.